ACS APPLIED MATERIALS & INTERFACES

Research Article

www.acsami.org

Methylene Blue Doped Films of Wool Keratin with Antimicrobial Photodynamic Activity

Annalisa Aluigi,*[,†] Giovanna Sotgiu,*[,†] Armida Torreggiani,[†] Andrea Guerrini,[†] Viviana T. Orlandi,[‡] Franco Corticelli,[§] and Greta Varchi[†]

[†]Institute for Organic Synthesis and Photoreactivity, National Research Council, via P. Gobetti, 101, 40129 Bologna, Italy

[‡]Department of Theoretical and Applied Sciences, University of Insubria, via J.H. Dunant 3, 21100 Varese, Italy

[§]Institute for Microelectronics and Microsystems, National Research Council, via P. Gobetti, 101, 40129 Bologna, Italy

ABSTRACT: In this work, keratin films doped with different amounts of methylene blue (MB) were developed in order to prepare new biodegradable and biocompatible materials for tissue engineering and wound healing, able to exert antimicrobial photodynamic activity upon irradiation with visible light. Preliminary results indicated that the swelling ratio, as well as the MB release, increases by increasing the pH. Moreover, the generation of reactive oxygen species (ROS) and singlet oxygen can be easily triggered and controlled by a fine-tuning of the irradiation time and MB concentration in the films. As concerns the photodynamic effects on keratin, the ROS attack does not induce any significant photodegradation on the protein, even if a slight photo-oxidation of sulfonated amino acids occurs. Finally, the film with the highest MB concentration (400 μg per gram of keratin) displays a significant photobactericidal activity against *Staphylococcus aureus* with a bacterial reduction that increases by increasing the irradiation time. In particular, the irradiation of KFMB400 film incubated with *S. aureus* at a concentration of 10^8 cfu mL^{-1} determined the 99.9% killing rate and the killing effect increased proportionally with irradiation time.

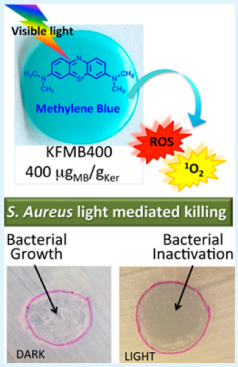

KEYWORDS: *keratin, film, antimicrobial photodynamic therapy, protein damage, methylene blue*

1. INTRODUCTION

When mats are engineered for wound healing, tissue engineering or drug delivery, natural polymers are preferred to synthetic ones, due to their biodegradability, their better biocompatibility, low immunogenicity and clinical functionality. Other advantages of natural polymers include high hydrophilicity as well as enhancement of cell adhesion and proliferation. The most common natural polymers used for biomedical applications are collagen, gelatin, hyaluronic acid, silk fibroin,[1] chitosan, alginate,[2] etc. However, among the biopolymers, keratin is the most abundant protein in nature, being the major component of wool, feather, hair, horns and nails, with promising applications in the biomedical field.[3] At the molecular level, keratin can be distinguished from other proteins, as fibroin or collagen, by the high amount of sulfur-containing amino acid cysteine (7−20% number of total amino acid residues).[4] Despite it can be recovered from low cost and renewable sources as poor quality raw wool and feather from butchery, keratin has only recently been studied as a potential material for biomedical applications. This is probably due to the fact that the technologies required to regenerate keratin from natural sources, while preserving molecular weights, conformation and biological functions, required extensive researches.[5] However, in the last years, keratin extracted from hair and wool has been utilized to produce several structures including sponges,[6] electrospun fibers[7] and films[8] as scaffolds for tissue engineering, wound dressings and drug-delivery systems. Keratin is attractive for such biomedical and regenerative medicine applications not only for its biodegradability and biocompatibility, but also because, similar to collagen, keratin contains the Arg-Gly-Asp and the Leu-Asp-Val cell adhesion amino sequences (cell binding motives) in its primary structure.[9]

A high level of antibacterial functionality is a desirable property for applications in wound healing and tissue engineering. Moreover, new antibacterial strategies are required to eradicate emerging multidrug-resistant bacteria.[10] In this regard, antimicrobial photodynamic therapy (APDT) represents a very promising alternative to traditional chemotherapy based on antibiotics. APDT combines the use of visible light, photosensitizers (PSs) and oxygen to induce the formation of singlet oxygen and other reactive oxygen species, able to kill bacteria. The principle on which the PDT operates is that the PS excited by exposure to low-power visible light at a specific wavelength reacts with oxygen through two pathways known as type I and type II reactions. In the type I mechanism, the excited PS reacts with bio-organic molecules producing reactive oxygen species (ROS), such as superoxide, hydroxyl radicals and hydrogen peroxide; whereas the type II reaction is accompanied by an energy transfer from the excited PS to molecular oxygen resulting in the generation of excited state singlet oxygen ($^1O_2$). The active products of both reactions

Received: May 29, 2015
Accepted: July 21, 2015
Published: July 21, 2015

DOI: 10.1021/acsami.5b04699
ACS Appl. Mater. Interfaces 2015, 7, 17416−17424

induce damage to biological targets, including bacterial and virus death.[11]

Among the commercially available photosensitizers, methylene blue (MB) has been recognized as very effective for antimicrobial treatment. MB has a maximum adsorption peak at 650 nm and it shows considerable antibacterial activity even when its exposure to light is limited.[12] Several microorganisms including Gram-positive and Gram-negative bacteria are known to be photoinactivated by MB.[13] Moreover, because MB does not need to penetrate or to come in contact with the bacteria to be effective,[14] its immobilization on a solid matrix offers several advantages over its use in solution. Indeed, the immobilized MB can be easily removed at the end of treatment, whereas being more resistant to bleaching as compared to free MB. Moreover, it can be reused several times without loosing its efficacy.[15] Several methods have been proposed for MB immobilization in a solid matrix: MB can be incorporated or adsorbed onto the matrix or it can be bonded to the matrix through ionic or covalent bonds.[16] MB has been incorporated into several polymer matrix such as silicone,[17] polyurethane[18] and polyethylene.[19] In the present work, different amount of MB were embedded into wool keratin films prepared by solvent casting. The photoactivity of MB-doped keratin films was evaluated first in solution containing photo-oxidable substrates and then against *Staphylococcus aureus* chosen as Gram-positive bacterium representative of skin infections.[20] Moreover, in order to evaluate if keratin is a suitable matrix for MB, the effects of ROS and $^1O_2$ on primary and supermolecular structures of the protein were investigated.

2. MATERIALS AND METHODS

2.1. Materials. Australian Merino wool was kindly supplied by Cariaggi Fine Yarns, S.p.a. The Mini Protean 3 Cell system, precast polyacrilamide gels and Coomassie Brilliant blue G 250 stain were purchased from Bio-Rad, whereas all other chemicals were purchased from Sigma-Aldrich.

2.2. Preparation and Characterization of Keratin Films Doped with Methylene Blue. Keratin was extracted from Merino wool (21 μm fineness) by sulphitolysis reaction, slightly modifying the extraction method described in a previous work.[21] Briefly, a fiber sample, withdrawn from a combed sliver and cleaned by Soxhlet extraction with petroleum ether, was washed with distilled water and dried at 21 °C and 60% relative humidity overnight.

Afterward, cleaned fibers (5 g) were cut into snippets and dispersed in 100 mL of aqueous solution containing urea (8 M), sodium metabisulphite (0.5 M) and sodium dodecyl sulfate (SDS, 0.1 M), under mechanical shaking at 65 °C overnight. The mixture was filtered with a vacuum filter (10−16 μm cutoff), dialyzed against distilled water using a cellulose tube (molecular weight cutoff 12−14 kDa) for 3 days at room temperature, changing the distilled water four times a day. The resulting aqueous solution was freeze-dried in order to obtain pristine keratin powder. Keratin solutions were prepared by dissolving the powder in pure formic acid at a final concentration of 15 wt %, under shaking, at room temperature, overnight. Afterward, the keratin solutions were doped with the desired amount of MB and were cast at room temperature overnight in polypropylene molds having a circular shape with diameter of 1.9 cm and thickness of 0.3 mm, in order to obtain MB-doped keratin films. Three kinds of films were prepared: undoped and doped keratin films (KF) with 50 μg (KFMB50) and 400 μg (KFMB400) of MB per gram of keratin.

Adsorption spectra of the films were acquired with a UV−vis spectrophotometer Cary 100 (Agilent Technologies). Films were fixed in the inner wall of a quartz cuvette and the absorbance in the 200−800 nm range was recorded using the undoped keratin film as a reference.

For the determination of the swelling ratio and the MB release, the doped films, completely dried (50 °C for 24 h), were immersed in phosphate buffers at pH values of 4.9, 7.4 and 10, at a liquor ratio of 5:1 and at 37 °C, overnight. Afterward, the films were taken out of the buffer, wiped dry with blotting paper and weighted immediately. The swelling ratio of the films were determined with the gravimetric test, as follows

$$\text{swelling ratio } (\%) = \frac{W_w - W_d}{W_d} \times 100 \quad (1)$$

where W_w (g) and W_d (g) are the weights of the wet and dry films, respectively.

To evaluate the MB release from the films, the MB concentration in the buffers was determined through the adsorption band at 650 nm by the calibration curve of MB in the buffers.

2.3. ROS and $^1O_2$ Generation. For the detection of ROS generation, each film of about 30 mg, was immersed in a well containing dichloro-dihydro-fluorescein (DHCF) dissolved in phosphate buffer (pH7.4) at 13 μM of concentration and they were irradiated several times with a tungsten lamp (Philips; 300W) at 20 cm from the films. Moreover, for each irradiation cycle, the DHCF solution was replaced with a freshly prepared one, as well as different irradiation times were used, e.g., 5, 10 and 15 min.

The generation of $^1O_2$ by films irradiation was determined by the 9,10-dimethylanthracene (DMA) method. Practically, quartz cells (2 mL) having a 1 cm path length and containing a solution of DMA (35 μM) in dimethylformamide (DMF) and the keratin film (about 5 mg) were irradiated with a tungsten lamp (Philips; 300W) for different irradiation times. The UV−vis spectra were acquired in the 200−800 nm range and kinetics of DMA photo-oxidation were studied following the decrease of the absorbance (A) at 378 nm. The observed kinetic constants (k_{obs}) were obtained from the slope calculated through the linear least-squares fit of the $\ln(A_0/A)$ vs time semilogarithmic plot.

2.4. Structural Analysis of Keratin Films. The morphological, structural and conformational changes of keratin films, eventually induced by ROS and $^1O_2$ production, were studied by scanning electron microscopy (SEM), polyacrylamide gel electrophoresis (SDS-PAGE) and Raman infrared spectroscopy. Analysis were carried out on films immersed in water and irradiated for 25 min using the nonirradiated film as a reference. In particular, the morphology of the films was analyzed with a Zeiss EVO LS 10 LaB6 scanning electron microscopy (SEM) instrument with an acceleration voltage of 5 kV and a working distance of 5 mm. The samples were mounted on aluminum specimens stubs with a double-side adhesive tape, sputtered with a gold layer for 1 min before the analysis.

The molecular weight distribution of the proteins was determined by SDS-PAGE according to Laemmli's method.[22] Samples were dissolved at a concentration of 15 mg/mL, a buffer solution contatining Tris/HCl (550 mM, pH 8.6), dithiothreitol (DTT, 140 mM) and urea (8 M). The dissolution was carried out under nitrogen atmosphere, overnight.[23] The protein solutions were then diluted to 7.5 mg/mL with the denaturing buffer containing 150 mg of sodium dodecyl sulfate, 0.5 mL of Tris−HCl (0.5M, pH 8.6), 1 mL of bromophenol blue (0.5 mg/mL) and glycerine 87% up to 4 mL, and heated at 70 °C for 5 min. The prepared solutions were run in a 12% polyacrilamide precasting gel, using a Mini Protean 3 Cell system from Bio-Rad at a constant voltage of 200 kV for 1 h. Proteins were visualized by Coomassie Brilliant blue G 250 stain using pristine freeze-dried keratin powder as molecular weight reference sample. The oxidation phenomena and the structural changes possibly induced on keratin by ROS and singlet oxygen were revealed by Raman analysis. One of the greatest advantages of Raman spectroscopy is the lack of sample preparation needed prior to analysis. Because Raman scatter originates from the surface of a sample (typically no deeper than several hundred micrometers), there is no concern with sample thickness, size or shape, so the analysis were carried directly out on films before and after ROS and $^1O_2$ attack. Because the damages caused by ROS mainly occur at the film surface, Raman analysis is a good tool for evaluating them. Moreover, to evaluate not only the

DOI: 10.1021/acsami.5b04699
ACS Appl. Mater. Interfaces 2015, 7, 17416−17424

damages occurring at the protein surface but also in the inner, the samples were fragmented and then analyzed. In this way, the Raman spectra resulted from the mean of the surface and inner damaged states. Fourier transform Raman spectra were recorded on a Bruker IFS 66 spectrometer equipped with a FRA-106 Raman module and a cooled Ge-diode detector. The excitation source was a Nd^{3+}-YAG laser (1064 nm), the spectral resolution was 4 cm^{-1} and the total number of scans for each spectrum were 4000. The laser power on the sample was about 100 mW. The curve fitting analysis was implemented using the OPUS/IR v 5.0 program, which uses the Levenberg–Marquardt algorithm. To fit the vibrational bands, some parameters should be fixed or constrain within reasonable limits (i.e., number and position of all components). To obtain information regarding the number and position of the component peaks, smoothed fourth derivates with a 13-point Savitsky–Golay function were used. These band positions were used as the initial guess for the curve-fitting of the original spectra. The Raman component profiles were described as a linear combination of Gaussian and Lorentzian functions. The vibrational assignments of the band components were carried out on the basis of the literature data. Regarding the secondary structure, the α-helix content was calculated from the area of the components in the 1648–1658 cm^{-1}, whereas β-turns mainly gave rise to the bands in the 1639–1645 and 1680–1694 cm^{-1} regions, whereas the components in the 1670–1678 cm^{-1} range reflected the contribution from β-sheet conformation.[24] The content of secondary structure was calculated from the area of the individually assigned bands and expressed as a fraction of the total area of the bands.

2.5. Antimicrobial Photoinactivation Assays. *Staphylococcus aureus* (MSSA) ATCC 25293 was grown 24 h in Luria–Bertani (LB) broth under aerobic conditions at 37 °C. Cell suspensions were obtained by diluting overnight cultures in phosphate buffer (KH_2PO_4/K_2HPO_4 10 mM pH 7.4) to reach a cell density of ~10^8 cfu mL^{-1}. KF and KFMB400 films were transferred in a 12 well microplate inoculated with bacteria and were incubated in the dark or irradiated with a 500 W halogen-tungsten lamp (fluence rate of 48 mW cm^{-2}, considering the 400 nm of the whole width of the lamp emission spectrum) for 25, 50, 75 and 100 min corresponding to energy densities 70, 140, 210 and 280 J cm^{-2}, respectively. The lamp was placed at a distance of 20 cm above the sample and a 1.5 cm thick circulating water/glass filter was interposed to avoid overheating. A panel of controls was set for each experiment: KF film incubated in the dark, KF film irradiated and KFMB400 incubated in the dark. The PDT efficacy was evaluated as viable counts of bacterial suspensions collected after dark incubation or irradiation. Viable counts, expressed as colony forming units (cfu mL^{-1}), were estimated by a plate count technique: a volume (0.1 or 0.01 mL) of undiluted or serially diluted samples was plated on LB agar plates and incubated for 24 h at 37 °C. The experiment was performed three times.

For the "patch assay", cell suspensions obtained by diluting overnight cultures in PB to reach a cell density of ~10^5 cfu mL^{-1} were inoculated on LB agar by means of a sterile swab. KF and KFMB400 were placed on LB agar and dark incubated or irradiated for 75 min. The films were removed and bacterial growth was controlled after overnight incubation at 37 °C.

3. RESULTS AND DISCUSSION

3.1. Film Properties. During keratin extraction by a sulfitolysis process, cysteine disulfide bonds are cleaved by sulphite to give cysteine-S-sulfonated residues (Ker-S-SO_3^-), known as Bunte salts, and cysteine thiol (Ker-SH).[25] This cystein-S-sulfonated keratin is highly soluble in pure formic acid; in turn these solutions can be easily processed into films by casting or into nanofibers by electrospinning. Moreover, pure keratin films cast from formic acid show an increased amount of β-sheet structures that make them insoluble in water or physiological buffer.[26,27] For the aforementioned reasons, formic acid was used as solvent to prepare keratin cast films doped with methylene blue. Another advantage of S-sulfonated keratin is that it contains several amino acids with polar side residues such as aspartic and glutamic acids, as well as cystein-S-sulfonate residues, able to bind cationic species such as methylene blue.[28]

The MB-doped keratin films were visually transparent (Figure 1) and although the undoped film is colorless, the

Figure 1. Keratin films doped with different amounts of methylene blue: undoped (A) and doped with 50 μg (B) and 400 μg (C) per mg of keratin.

MB doped ones are homogeneously blue and the color intensity increases with increasing the MB concentration. Moreover, the hydrated films appear flexible and easy to handle (Figure 2).

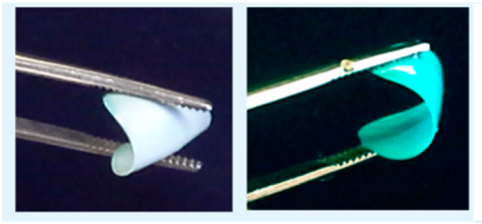

Figure 2. Free standing and flexible hydrated keratin films.

The spectral characteristics of keratin films doped with MB are shown in Figure 3. Compared to the adsorption wavelength

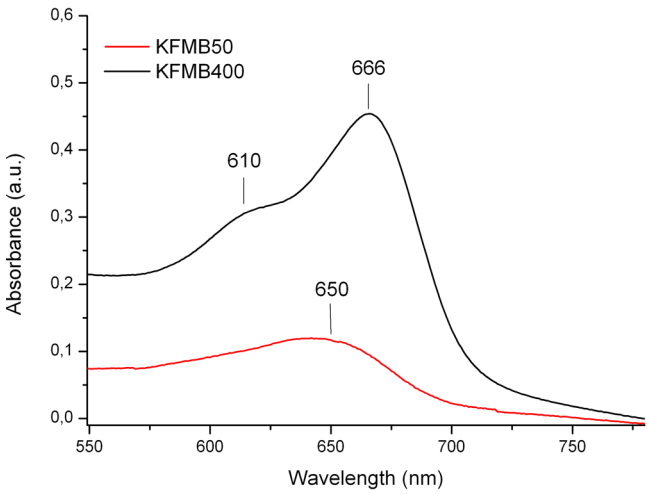

Figure 3. Adsorption spectra of the doped films in the 520–760 nm range.

(650 nm) of KFMB50, the adsorption of KFMB400 is shifted toward a longer wavelength (666 nm). Moreover, a noticeable peak at 610 nm was detected in the adsorption spectrum of KFMB400, indicating the formation of MB dimers,[29] probably due to the relatively high concentration of the dye with respect to keratin.

The swelling ability of a material is a very important parameter especially in wound healing; in fact, if the wound

DOI: 10.1021/acsami.5b04699
ACS Appl. Mater. Interfaces 2015, 7, 17416–17424

dressing has the ability to swell, it will give moisture to the wound, thereby contributing to better healing.[30] The swelling ratio of the films was found to be dependent on the environmental pH, indeed, whereas it was of about 160% at pH 4.9, it increased to 677% at pH 7.4 and to 849 at basic pH of 10 (Table 1). The lowest swelling ratio at a slight acid pH is due to the lower solubility of keratin in aqueous media near its isoelectric point (pH 4.5). Because swelling involves the transport of ions and small molecules between the fluid and the biomaterial, the same trend was observed for the MB release from the films that was negligible at pH 4.9 and increased with increasing the pH reaching the 61% at pH 10.

Table 1. Effect of pH on Swelling Ratio and MB Release of the Keratin Films

pH	swelling ratio (%)	MB release (%)
4.9	160 ± 34	
7.4	677 ± 61	20
10	849 ± 60	61

3.2. Effect of MB Concentration and Irradiation Time on ROS and $^1O_2$ Generation. The ROS generation induced by light irradiation of the MB-doped keratin films were detected using dichloro-dihydro-fluorescein (DHCF) as chemical probe. In this method, upon oxidation by ROS, the nonfluorescent DHCF is converted to the highly fluorescent 2′,7′-dichlorofluorescein (DCF), which can be detected through its absorption band at 500 nm. The intensity of the DCF absorption band is correlated to the quantity of generated ROS. The adsorption spectra of DCF generated in the solution containing MB doped keratin films after three irradiation cycles (5′, 10′ and 15′ irradiation time) are reported in Figure 4. As can be seen, the MB doped films maintain their photoactivity for different irradiation cycles giving a compelling evidence of their photostability. Moreover, the absorbance at 500 nm increases with increasing the irradiation time (Figure 4a,b,c), as well as with increasing the MB concentration (Figure 4d), thus confirming that ROS are generated more effectively with increasing the irradiation time and the MB doping in the films.[31] The little amount of ROS generated by irradiation of undoped keratin film (Figure 4a) can be ascribed to the presence of chromophoric amino acids as tryptophan (Trp), tyrosine (Tyr), phenylalanine (Phe), histidine (His) and cysteine/cystine (Cys) in the protein chain.

The $^1O_2$ generation from undoped and MB doped keratin films was evaluated by monitoring the change in the adsorption spectra of 9,10-dimethylanthracene (DMA) in DMF during the first 10 min of irradiation (Figure 5). In this system, the generated $^1O_2$ converts the substrate (DMA) into its corresponding endoperoxide form, leading to a reduction of intensity of the peak at 378 nm. The efficiency of $^1O_2$ production is represented by the k_{obs} obtained from the slope of the first-order kinetic plots shown in Figure 5. As can be seen in Table 2, also in this case, a slight photoactivity, stimulated by chromophoric amino acids of keratin, was observed for the undoped film. However, the highest k value is obtained for the film KFMB50. This behavior could be ascribed to the partial dimerization observed in the KFMB400 film (Figure 3), for

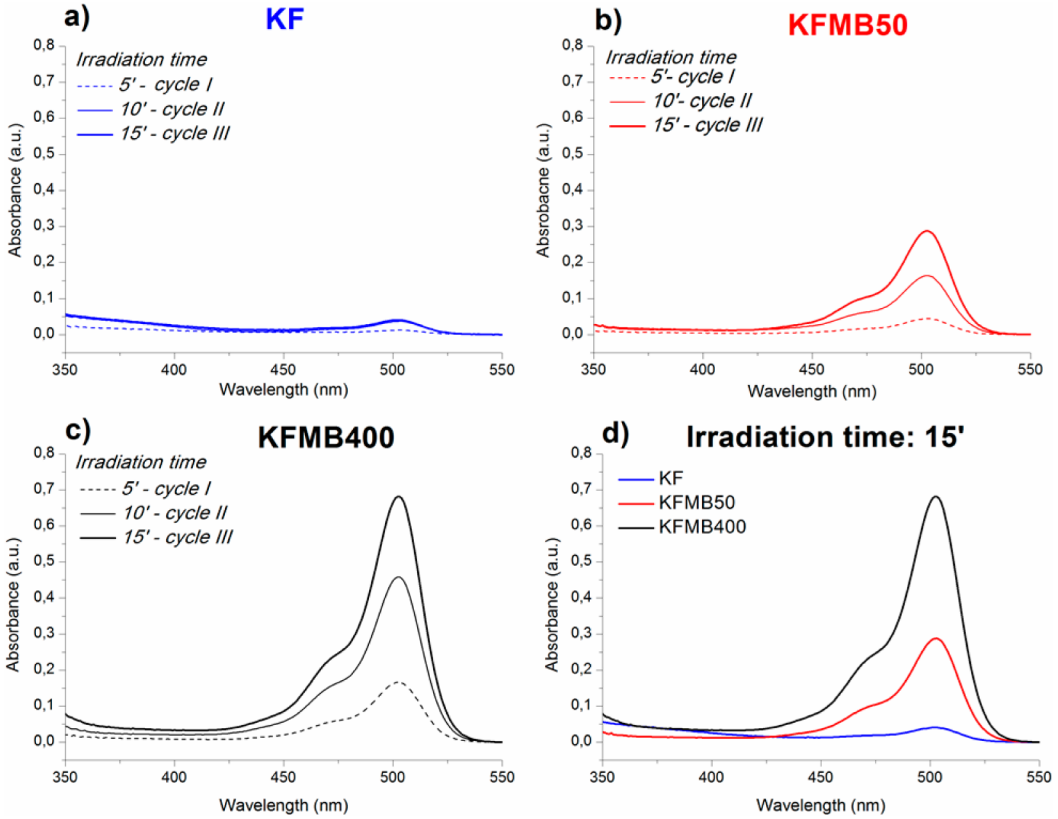

Figure 4. Adsorption spectra of 2′,7′-dichlorofluorescein (DCF) developed from different irradiation times of dichloro-dihydro-fluorescein (DHCF) in the presence of (a) KF, (b) KFMB50, (c) KFMB400 and (d) comparison of ROS generated upon 15′ irradiation of keratin films doped with different amounts of MB.

DOI: 10.1021/acsami.5b04699
ACS Appl. Mater. Interfaces 2015, 7, 17416−17424

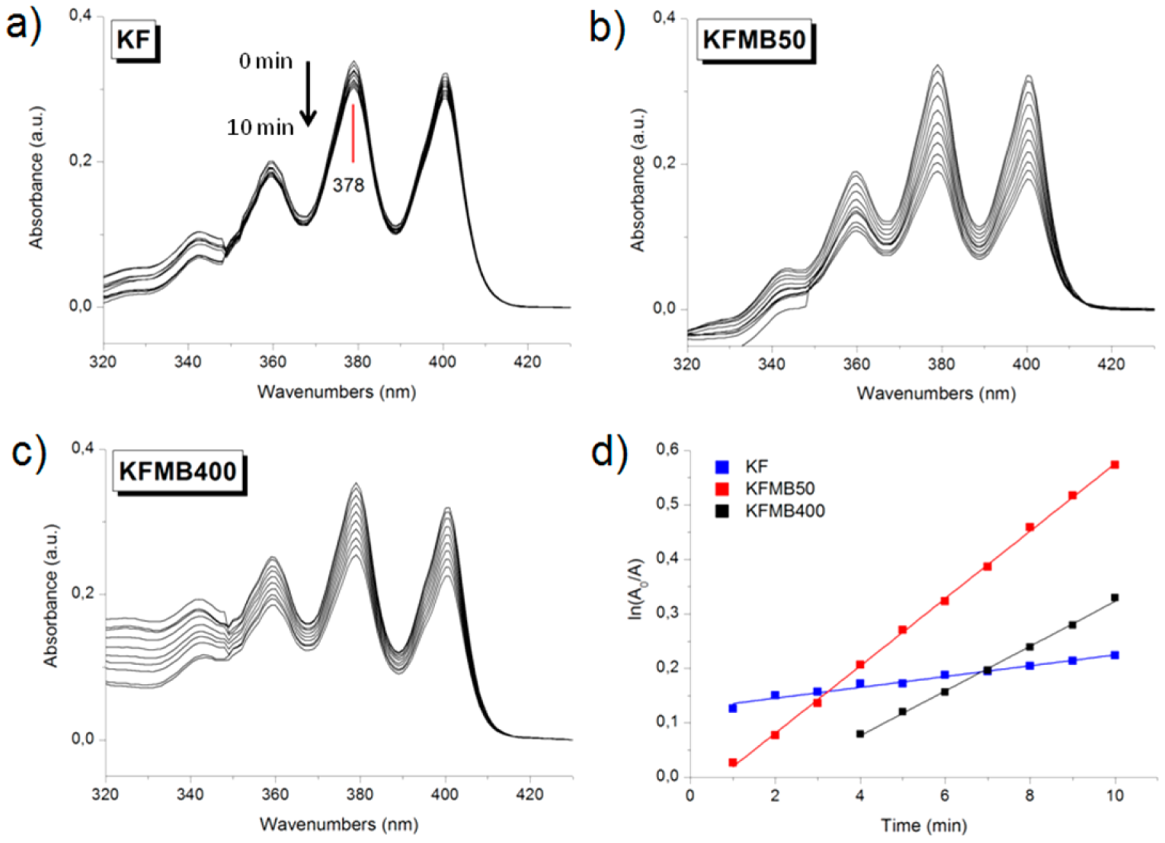

Figure 5. Adsorption spectra changes of DMA at different irradiation times (from 0 to 10 min) and photo-oxidized by keratin films with different MB concentrations (a, b and c) and first-order plots for the photo-oxidation of DMA by keratin films with different MB concentrations (d).

Table 2. Kinetic Constant (k) Values for Undoped and MB Doped Keratin Films

sample	k_{obs} (10^{-2}/min)
KF	0.99 ± 0.05
KFMB50	6.18 ± 0.06
KFMB400	4.10 ± 0.08

which the dimers could be responsible of a shift from the type II to type I photoreaction, thus reducing the $^1O_2$ generation.[32]

3.3. Evaluation of Keratin Damage Induced by ROS and $^1O_2$ Generation. To investigate the effect of MB doping, ROS and $^1O_2$ on the morphological characteristics of the films, the SEM image of pristine keratin film (Figure 6a) was compared with those of the film at higher MB concentrations (KFMB400), both nonirradiated (Figure 6b) and irradiated for 25 min (Figure 6c). The surface of pristine keratin film is homogeneous and without defects and neither the MB doping, nor the ROS and $^1O_2$ generation alter the films surface, which remains smooth and without cracks.

The photodegradation of keratin caused by ROS and $^1O_2$ was evaluated analyzing the protein molecular weights by means of electrophoresis SDS-PAGE. In particular, the molecular weights of pristine keratin were compared with those of the irradiated keratin films, both undoped and MB doped ones. As shown in Figure 7, the electrophoretic pattern of pristine keratin (Figure 7, lane 1), shows the two characteristic high-molecular-weight bands (60−45 kDa) associated with the low-sulfur intermediate filaments proteins

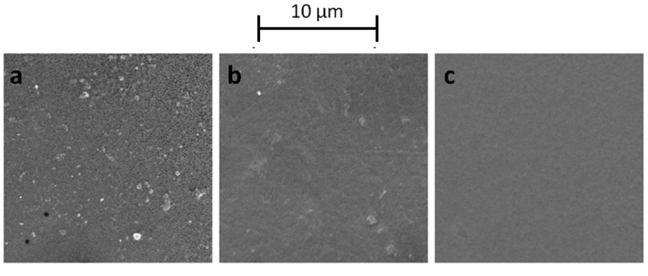

Figure 6. SEM images of (a) pristine keratin film, (b) nonirradiated KFMB400 and (c) KFMB400 irradiated for 25 min.

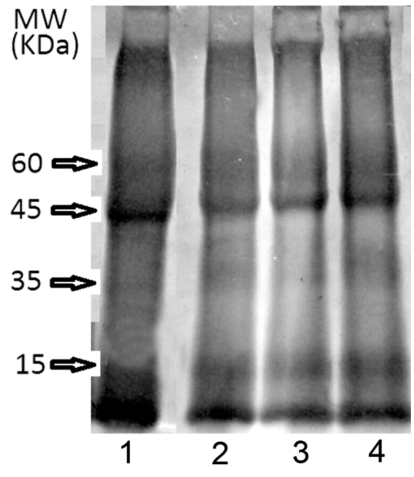

Figure 7. Electrophoresis SDS-PAGE gel of pristine keratin (lane 1) and irradiated KF (lane 2), KFMB50 (lane 3) and KFMB400 (lane 4).

DOI: 10.1021/acsami.5b04699
ACS Appl. Mater. Interfaces 2015, 7, 17416−17424

(IFPs) and several low-molecular-weight bands (35−15 kDa) attributed to the high sulfur (HSPs) proteins of the matrix.[25] The electrophoretic patterns of the irradiated films suggest that the protein, regardless the MB concentration, does not undergo photodegradation (Figure 7, lanes 2, 3 and 4).

To assess the main reactive sites for ROS and $^1O_2$ and their effects on protein photo-oxidation and folding, the Raman spectra of KFMB400 film were recorded before and after irradiation. Among the amino acid residues present, Cys is one of the most sensitive residues toward ROS- and singlet oxygen-induced oxidation. This conclusion was drawn out from the analysis of the Raman spectral region where the vibrations of sulfur-containing residues are visible (Figure 8). After the light

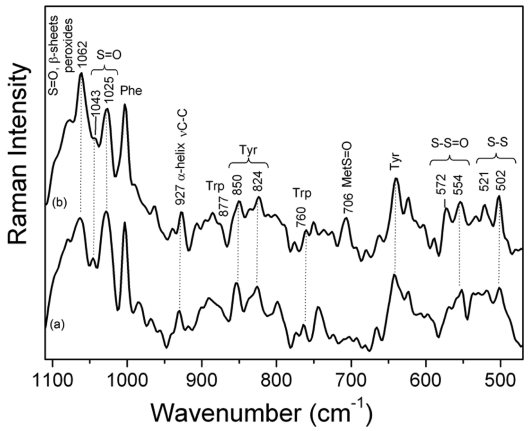

Figure 8. 1110−490 cm^{-1} Raman region of KFMB400 film (a) before and (b) after ROS and $^1O_2$ attack.

exposition, an increase in the bands at 572 and 554 cm^{-1}, due to the vibration modes of S—S═O and −SO_2—S, was visible indicating the formation of sulfur-containing oxidation products, such as disulfide-S-oxide (RSS(═O)R). The formation of some S-oxides was confirmed by the presence of the 1026 cm^{-1} band, due to the stretching vibration of S═O moiety (Figure 8).

Regarding Met residues, they are readily oxidized to Met sulfoxide (MetS═O) by ROS including $^1O_2$, as suggested by the presence of two Raman bands at 701 cm^{-1} and about 1040 cm^{-1} (Figure 8), considered a marker pattern of the formation of methionine sulfoxide.[33] In fact, the first one is characteristic of the C—S stretch from MetS═O, and the other is ascribable to the νS═O vibration.[34] Thus, the sulfur moiety in Met is another target of the radical species. Keratin contains Tyr and Trp residues that give rise to many Raman bands due to aromatic ring vibrations. Exposure of the protein to ROS led to changes in the bands of the aromatic side chains of these residues (i.e., 1621, 1550, 850, 824, etc., cm^{-1}), suggesting the occurrence of their radical-induced modifications on them[35] (Figures 8 and 9A). A qualitative evaluation of the conformational changes occurring upon ROS exposure was obtained by analyzing the bands of amides I (1640−1690 cm^{-1}) and III (1240−1305 cm^{-1}), whose wavenumbers are correlated with different protein conformations.[35,36] The position of the amide I band suggests that both β-sheets and β-turns structures are still present after irradiation treatment, although some spectral modifications are indicative of slight differences in the secondary structure contents (Figure 9A). In fact, the amide I band was still centered in the 1671−1665 cm^{-1} range even after light treatment, although shifted toward lower wavenumbers (from 1670 to 1667 cm^{-1}); on the other hand, the intensity of the amide III components in the 1320−1285 cm^{-1} region, due to β-turns vibrations, indicates the presence of the β-turn motifs before and after ROS exposure. The extent of modification induced by ROS and singlet oxygen to the secondary structure of the protein, was performed by curve fitting analysis of the Raman amide I band I (1640−1690 cm^{-1}). Although this method does not yield the absolute content of the secondary structures (because the effective intensities of the bands corresponding to different structure elements are not completely equivalent), it may be of value in probing the nature and the extent of structural changes in proteins induced by external factors interacting with protein molecules such as ligand binding, free radical attack or photo-oxidation.

The curve-fitting results, shown in Figure 9B, indicated that the ROS and $^1O_2$ attack toward keratin caused only small changes in the secondary structure contents. In fact, the main contribute to the protein folding (more than 80%) both before and after the irradiation comes from β-sheets and β-turns structures. However, the partial oxidation of keratin caused a loss in the β-sheets content and an small increase in the β-turns

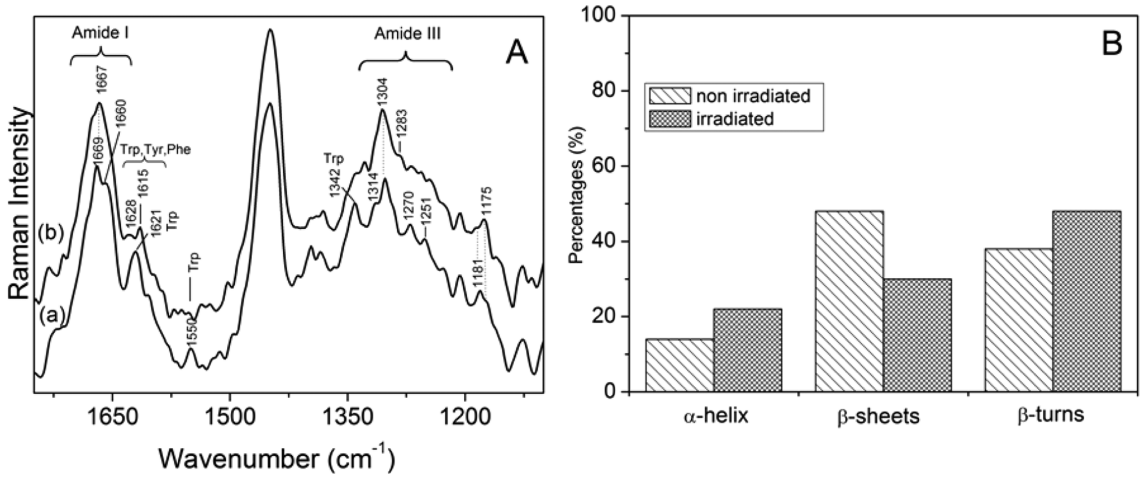

Figure 9. (A) 1770−1100 cm^{-1} Raman region of KFMB400 film (a) before and (b) after ROS and $^1O_2$ attack. (B) Block diagram of the secondary structures found in keratin before and after ROS exposure. The percentages were calculated by the analysis of the 1700−1640 cm^{-1} Raman region.

DOI: 10.1021/acsami.5b04699
ACS Appl. Mater. Interfaces 2015, 7, 17416−17424

motifs and α-helix amount. The latter change was confirmed by the slight intensity increase in the band at 930 cm^{-1} due to α-helix.

Because ROS and $^1O_2$ generation does not induce any protein photodegradation but only a slight oxidation of sulfonated amino acids, the characteristics cell binding motives of wool keratin are preserved after light irradiation of doped films.

3.4. Antibacterial Photodynamic Inactivation. *S. aureus* is successfully killed by PDT with PSs belonging to different family compounds,[37] but no study reports the photoinactivation of *S. aureus* by keratin films doped with PSs. In this study, it was evaluated, for the first time, the antimicrobial activity of keratin films doped with MB upon irradiation by a wide spectrum white light. The irradiation of KFMB400 film incubated with *S. aureus* at a concentration of 10^8 cfu mL^{-1} determined the 99.9% of killing rate and the killing effect increased proportionally with irradiation time (Figure. 10).

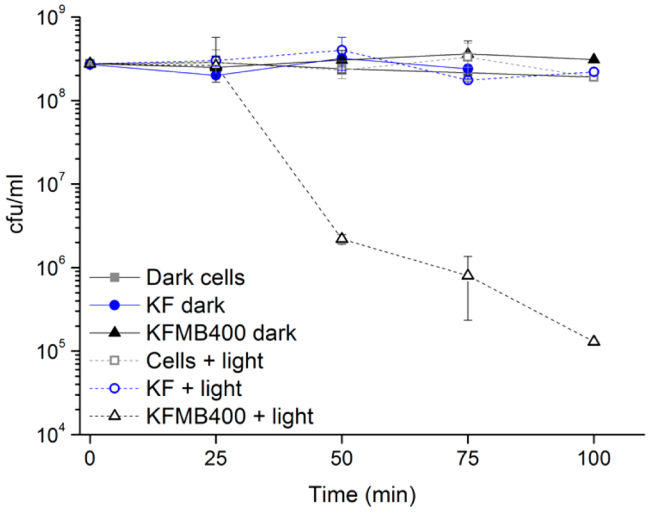

Figure 10. Effect of dark incubation on cell viability (cfu/mL) of *S. aureus* and *S. aureus* treated with KF and KFMB400 films; effect of irradiation on cell viability of *S. aureus* and *S. aureus* treated with KF and KFMB400 films.

Keratin films unloaded with MB were not toxic to cells either in the dark or upon irradiation and KFMB400 film incubated in the dark did not alter bacterial viability (Figure 10). To evaluate the possible contribution of free PS to the observed killing rate, photodynamic treatment was performed administering MB at a concentration equivalent to that released after 24 h of irradiation by the KFMB400 film. As *S. aureus* was not sensitive to this PDT treatment, it can be supposed that the observed killing effect was exclusively due to the photo-oxidative stress elicited by irradiated MB immobilized on the film. Furthermore, a certain degree of PS concentration dependent killing effect was observed, as in a preliminary experiment, irradiation of KFMB50 film caused a killing rate lower than that obtained with irradiation of KFMB400 one (data not shown).

To reproduce a scenario more similar to an *in vivo* application, an antimicrobial "patch assay" was performed. As shown in Figure 11, the incubation in the dark of KFMB400 film did not determine a killing effect as bacterial growth was clear (Figure 11 A). On the other hand, the irradiation of KFMB400 film killed cells inoculated on LB agar and prevented colonies growth (Figure 11B).

4. CONCLUSION

In the present work, photoactive keratin films made of keratin extracted from wool and doped with two different amounts of methylene blue were proposed as novel biomatrices for tissue engineering or wound healing purposes. The adsorption spectra of the films in the UV−vis region indicated that the methylene blue is mainly embedded as a monomer, even if the presence of dimers can be detected in the films at the highest MB concentration (400 μg of MB per gram of keratin). The swelling ratio, as well as the MB release have been demonstrated to increase with increasing the pH. Concerning the film photochemical properties, the results showed that the ROS generation is dependent on both photosensitizer concentration and time of irradiation. On the other hand, the efficiency of $^1O_2$ production is lower for the films containing the highest amount of MB and this is probably due to the presence of dimers causing a shift from the type II to type I reaction. The evaluation of protein damage eventually induced by ROS and singlet oxygen generation showed that any photodegradation occurs suggesting that keratin represents a solid biocompatible and biodegradable support for photodynamic therapy treatments. However, a slight oxidation of sulfur containing amino acids (cysteine and methionine) and a slight loss in the β-sheets content was detected. Moreover, the KFMB400 film showed a 99.9% killing rate against *S. aureus* upon irradiation with visible light, and the killing effect increased proportionally with irradiation time. Future investigations will be addressed to the photoinactivation of *Pseudomonas aeruginosa*, a Gram-negative microorganisms that showed to be particularly tolerant to photodynamic treatment.

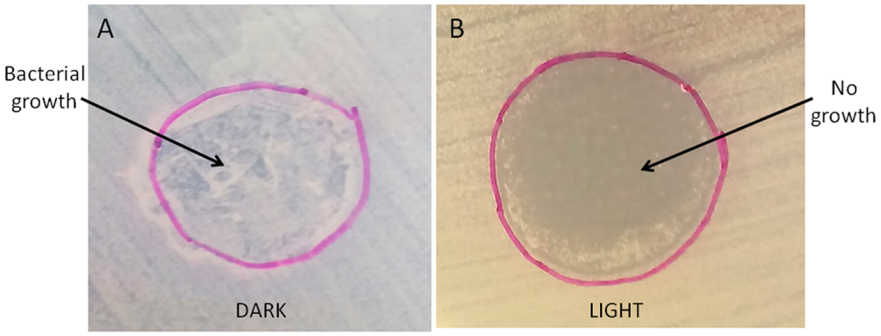

Figure 11. Antimicrobial "patch assay". KFMB400 film placed upon LB agar inoculated with *S. aureus* was incubated in the dark (A) or irradiated (B) for 75 min. After film removal bacteria growth 24 h at 37 °C.

DOI: 10.1021/acsami.5b04699
ACS Appl. Mater. Interfaces 2015, 7, 17416−17424

AUTHOR INFORMATION

Corresponding Authors

*Annalisa Aluigi. E-mail: annalisa.aluigi@isof.cnr.it. Fax: +39 0516398349. Tel.: +39 0516398326.

*Giovanna Sotgiu. E-mail: giovanna.sotgiu@isof.cnr.it. Fax: +39 0516398349. Tel.: +39 0516398290.

Notes

The authors declare no competing financial interest.

ACKNOWLEDGMENTS

The authors acknowledge Cariaggi Fine Yarns, S.p.a., for the merino wool fibers supply.

REFERENCES

(1) Zhou, J.; Zhang, B.; Shi, L.; Zhong, J.; Zhu, J.; Yan, J.; Wang, P.; Cao, C.; He, D. Regenerated Silk Fibroin Films with Controllable Nanostructure Size and Secondary Structure for Drug. *ACS Appl. Mater. Interfaces* **2014**, *6* (24), 21813−21821.

(2) Agrawal, P.; Soni, S.; Mittal, G.; Bhatnagar, A. Role of Polymeric Biomaterials as Wound Healing Agents. *Int. J. Lower Extremity Wounds* **2014**, *13* (3), 180−190.

(3) Fraser, R. D. B.; MacRae, T. P.; Rogers, G. E. Properties of Solubilized Keratins. In *Keratins: Their Composition, Structure, and Biosynthesis*; Charles C Thomas: Springfield, IL, 1972; pp 30−55.

(4) Dawling, L. M.; Crewther, W. G.; Parry, A. D. Secondary Structure of Component 8c-1 of Alpha-Keratin. An Analysis of the Amino Acid Sequence. *Biochem. J.* **1986**, *236* (3), 750−712.

(5) Aboushwareb, T.; Eberli, D.; Ward, C.; Broda, C.; Holcomb, J.; Atala, A.; Van Dyke, A. A Keratin Biomaterial Gel Haemostat derived from Human Hair: Evaluation in a Rabbit Model of Lethal Liver Injury. *J. Biomed. Mater. Res., Part B* **2009**, *90* (1), 45−54.

(6) Hamasaki, S.; Tachibana, A.; Tada, D.; Yamauchi, K.; Tanabe, T. Fabrication of Highly Porous Keratin Sponges by Freeze-Drying in the Presence of Calcium Alginate Beads. *Mater. Sci. Eng., C* **2008**, *28* (8), 1250−1254.

(7) Xu, H.; Cai, S.; Xu, L.; Yang, Y. Water-Stable Three-Dimensional Ultrafine Fibrous Scaffolds from Keratin for Cartilage Tissue Engineering. *Langmuir* **2014**, *30*, 8461−8470.

(8) Borrelli, M.; Joepen, N.; Reichl, S.; Finis, D.; Schoppe, M.; Geerling, G.; Schrader, S. Keratin Films for Ocular Surface Reconstruction: Evaluation of Biocompatibility in an *in-Vivo* Model. *Biomaterials* **2015**, *42*, 112−120.

(9) Rouse, J. G.; Van Dyke, M. E. A Review of Keratin-Based Biomaterials for Biomedical Applications. *Materials* **2010**, *3*, 999−1014.

(10) Huttner, A.; Harbarth, S.; Carlet, J.; Goossens, H.; Homes, A.; Jarlier, V.; Voss, A.; Pittet, D. Antimicrobial Resistance: a Global View from the 2013 World Healthcare-Associated Infections Forum. *Antimicrob. Resist. Infect. Control* **2013**, *2* (31), 1−13.

(11) Dai, T.; Huang, Y. Y.; Hamblin, M. R. Photodynamic Therapy for Localized Infections − State of the Art. *Photodiagn. Photodyn. Ther.* **2009**, *6*, 170−88.

(12) Wainwright, M.; Crossley, K. B. Methylene Blue − a Therapeutic Dye for All Seasons? *J. Chemother.* **2002**, *14*, 431−443.

(13) Usacheva, M. N.; Teichert, M. C.; Biel, M. A. Comparison of the Methylene Blue and Toluidine Blue Photobactericidal Efficacy against Gram-Positive and Gram-Negative Microorganisms. *Lasers Surg. Med.* **2001**, *29*, 165−173.

(14) Dahl, T. A.; Middenad, W. R.; Hartman, P. E. Pure Singlet Oxygen Citotoxycity for Bacteria. *Photochem. Photobiol.* **1987**, *46*, 345−352.

(15) Paczkowski, J.; Neckers, D. C. Photochemical Properties of Rose Bengal 11 Fundamental Studies in Heterogeneous Energy Transfer. *Macromolecules* **1985**, *18*, 2412−2418.

(16) Nowakowska, M.; Pezynsky, M. K.; Browska, M. D. Polymeric Photosensitizers, 5 Synthesis and Photochemical Properties of Poly[(N-isopropylacrylamide)-co-(vinylbenzyl chloride)] Containing Covalently Bound Rose Bengal Chromophores. *Macromol. Chem. Phys.* **2001**, *202*, 1679−1688.

(17) Piccirillo, C.; Perni, S.; Gil-Thomas, J.; Prokopovich, M.; Wilson, M.; Pratten, J.; Parkin, I. P. Antimicrobial Activity of Methylene Blue and Toluidine Blue O Covalently Bound to a Modified Silicone Polymer Surface. *J. Mater. Chem.* **2009**, *19*, 6167−6171.

(18) Naik, A. J. T.; Ismail, S.; Kay, C.; Wilson, M.; Parkin, I. P. Antimicrobial Activity of Polyurethane Embedded with Methylene Blue, Toluidine Blue and Gold Nanoparticles against *Staphilococcus aureus;* Illuminated with White Light. *Mater. Chem. Phys.* **2011**, *129*, 446−450.

(19) Cahan, R.; Schwartz, R.; Langzam, Y.; Nitzan, Y. Light-Activated Antibacterial Surfaces Comprise Photosensitizers. *Photochem. Photobiol.* **2011**, *87*, 1379−1386.

(20) Saeed, K.; Marsh, P.; Ahmad, N. Cryptic Resistance in *Staphylococcus Aureus*: a Risk for the Treatment of Skin Infection? *Curr. Opin. Infect. Dis.* **2014**, *27* (2), 130−136.

(21) Aluigi, A.; Tonetti, C.; Tonin, C.; Casasola, R.; Ferrero, F. Wool Keratin Nanofibres for Copper (II) Adsorption. *J. Biobased Mater. Bioenergy* **2012**, *6*, 230−236.

(22) Laemmli, U. K. Cleavage of Structural Proteins During the Assembly of the Head Bacteriophage T4. *Nature* **1970**, *227*, 680−685.

(23) Marshall, R. C. Analysis of the Proteins form Single Wool Fiber by Two-Dimensional Polyacrilamide Gel Electrophoresis. *Text. Res. J.* **1981**, *51*, 106−108.

(24) Wojciechowska, E.; Włochowicz, A.; Wesełucha-Birczyńska, A. Application of Fourier-Transform Infrared and Raman Spectroscopy to Study Degradation of the Wool Fiber Keratin. *J. Mol. Struct.* **1999**, *511−512*, 307−318.

(25) Maclaren, J. A.; Milligan, B. *Wool Science: The Chemical Reactivity of the Wool Fibre*; Science Press, Marrickville, Australia, 1981.

(26) Aluigi, A.; Zoccola, M.; Vineis, C.; Tonin, C.; Ferrero, F.; Canetti, M. Study on the Structure and Properties of Wool Keratin Regenerated from Formic Acid. *Int. J. Biol. Macromol.* **2007**, *41* (3), 266−273.

(27) Vasconcelos, A.; Freddi, G.; Cavaco-Paulo, A. Biodegradable Materials Based on Silk Fibroin and Keratin. *Biomacromolecules* **2008**, *9*, 1299−1305.

(28) Aluigi, A.; Rombaldoni, F.; Tonetti, C.; Jannoke, L. Study on Methtylene Blue Adsorption on Keratin Nanofibrous Membranes. *J. Hazard. Mater.* **2014**, *268*, 156−165.

(29) Golz, E. K.; Vander Griend, D. A. Modeling Methylene Blue Aggregation in Acidic Solution to the Limits of Factor Analysis. *Anal. Chem.* **2013**, *85*, 1240−1246.

(30) Enoch, S.; Leaper, D. J. Basic Science and Wound Healing. *Surgery* **2008**, *26*, 31−37.

(31) Davies, M. J. Singlet Oxygen-Mediated Damage to Proteins and its Consequences. *Biochem. Biophys. Res. Commun.* **2003**, *305*, 761−770.

(32) Junqueira, H. C.; Severino, D.; Dias, L. G.; Gugliotti, M.; Baptista, M. S. Modulation of the Methylene Blue Photochemical Properties Based on the Adsorption at Aqueous Micelle Interfaces. *Phys. Chem. Chem. Phys.* **2002**, *4*, 2320−2328.

(33) Torreggiani, A.; Barata-Vallejo, S.; Chatgilialoglu, C. Combined Raman and IR Spectroscopic Study on the Radical-Based Modifications of Methionine. *Anal. Bioanal. Chem.* **2011**, *401*, 1231−1239.

(34) Ravi, J.; Hills, A. E.; Cerasoli, E.; Rakowska, P. D.; Ryadnov, M. G. FTIR Markers of Methionine Oxidation for Early Detection of Oxidized Protein Therapeutics. *Eur. Biophys. J.* **2011**, *40*, 339−345.

(35) Jurasekova, Z.; Marconi, G.; Sanchez-Cortes, S.; Torreggiani, A. Spectroscopic and Molecular Modeling Studies on the Binding of the Flavonoid Luteolin and Human Serum Albumin. *Biopolymers* **2009**, *91*, 917−927.

(36) Jurasekova, Z.; Tinti, A.; Torreggiani, A. Use of Raman Spectroscopy for the Identification of Radical-Mediated Damages in Human Serum Albumin. *Anal. Bioanal. Chem.* **2011**, *400*, 2921−2931.

(37) Fu, X. J.; Fang, Y.; Yao, M. Antimicrobial Photodynamic Therapy for Methicillin-Resistant *Staphylococcus aureus* Infection.

DOI: 10.1021/acsami.5b04699
ACS Appl. Mater. Interfaces 2015, 7, 17416−17424

BioMed Res. Int. **2013**, *2013*, art. no. 159157, DOI: 10.1155/2013/159157.

DOI: 10.1021/acsami.5b04699
ACS Appl. Mater. Interfaces 2015, 7, 17416−17424